

Supporting Information

Elastic Properties of Van Der Waals Epitaxy Grown Bismuth Telluride 2D Nanosheets

Lingling Guo,^{1,2} Haoming Yan,^{1,2} Quentarius Moore,³ Michael Buettner,² Jinhui Song,^{2,4} Lin Li,^{2,4} Paulo T. Araujo,^{2,5} and Hung-Ta Wang^{1,2,a)}

¹Department of Chemical and Biological Engineering, The University of Alabama, Tuscaloosa, AL 35487, USA

²Center for Materials for Information Technology (MINT Center), The University of Alabama, Tuscaloosa, AL 35487, USA

³Department of Chemistry and Biochemistry, Jackson State University, Jackson, MS 39217, USA

⁴Department of Metallurgical and Materials Engineering, The University of Alabama, Tuscaloosa, AL 35487, USA

⁵Department of Physics and Astronomy, The University of Alabama, Tuscaloosa, AL 35487, USA

a) Author to whom correspondence should be addressed. Electronic mail: htwang@eng.ua.edu

List of content:

1. Van der Waals epitaxy of Bi₂Te₃ 2D nanosheets
2. Microfabrication of porous SiO₂/Si substrates
3. 2D nanosheets transfer and suspension
4. Calibrations of AFM cantilever spring constants
5. AFM tip radius measurements
6. List of the data reported
7. References cited

1. Van der Waals epitaxy of Bi₂Te₃ 2D nanosheets

The Bi₂Te₃ 2D nanosheets were synthesized via the van der Waals epitaxy process, as previously reported by Li *et al.*¹ A schematic of the vapor phase reaction system is shown in **Figure S1**. In a typical setup, the source material, Bi₂Te₃ powder (~99.98%, from Alfa Aesar), was loaded in a ceramic boat and placed in the center of the horizontal tube furnace (1 inch in diameter). The mica substrate (Muscovite mica, V3, from Electron Microscopy Sciences) was trimmed (~2×4 cm), cleaved, and immediately placed in the downstream location of the furnace tube, 12-16 cm away from the Bi₂Te₃ source. The van der Waals epitaxy processes were carried out for 0.5~3 hours, with a source temperature of 450~480 °C and a pressures ranging of 20~50 torr, using Argon (20 SCCM, high purity, from Airgas) as the carrying gas.

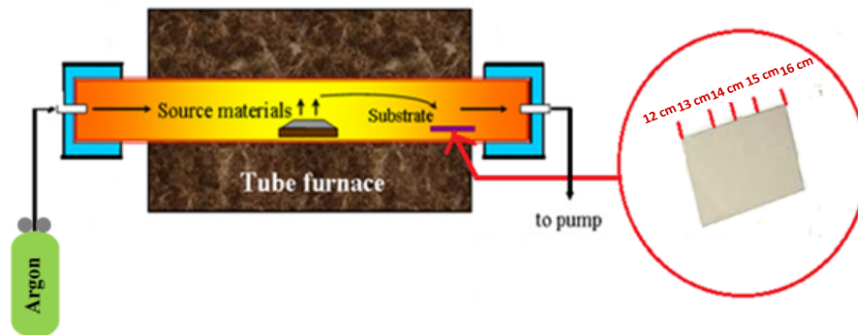


Figure S1. Schematic illustration of the reaction system.

Owing to the fact that there is a temperature gradient along the tube furnace (*i.e.*, along the mica substrate), the morphologies of the Bi₂Te₃ 2D nanosheets are very sensitive to the growth location. By tuning above-mentioned growth parameters, it was found that the optimal position was $\sim 13.5 \pm 0.3$ cm away from the Bi₂Te₃ source, resulted in thicknesses of 2~25 nm and lateral sizes of 5~100 μm . The size of the Bi₂Te₃ 2D nanosheets was dominantly affected by the growth temperature and the Bi₂Te₃ vapor pressure parameters, which is consistent with

literature.¹ We carried out a statistical analysis of thickness *vs.* lateral size distribution of the circular (31 samples) and triangular nanosheets (28 samples) for the optimized parameters (growth time = 60 mins, pressure = 23 torr, and source temperature = 474 °C). Two sample locations, the upstream area (primarily triangular nanosheets) and the downstream area (primarily circular nanosheets), were characterized. **Figure S2** presents the statistical analysis, showing that the thicknesses of the circular 2D nanosheets (3~8 nm) are thinner than those of the triangular 2D nanosheets (7~26 nm); the lateral sizes of the circular 2D nanosheets (2~9 μm) are also smaller than those of the triangular 2D nanosheets (6~17 μm).

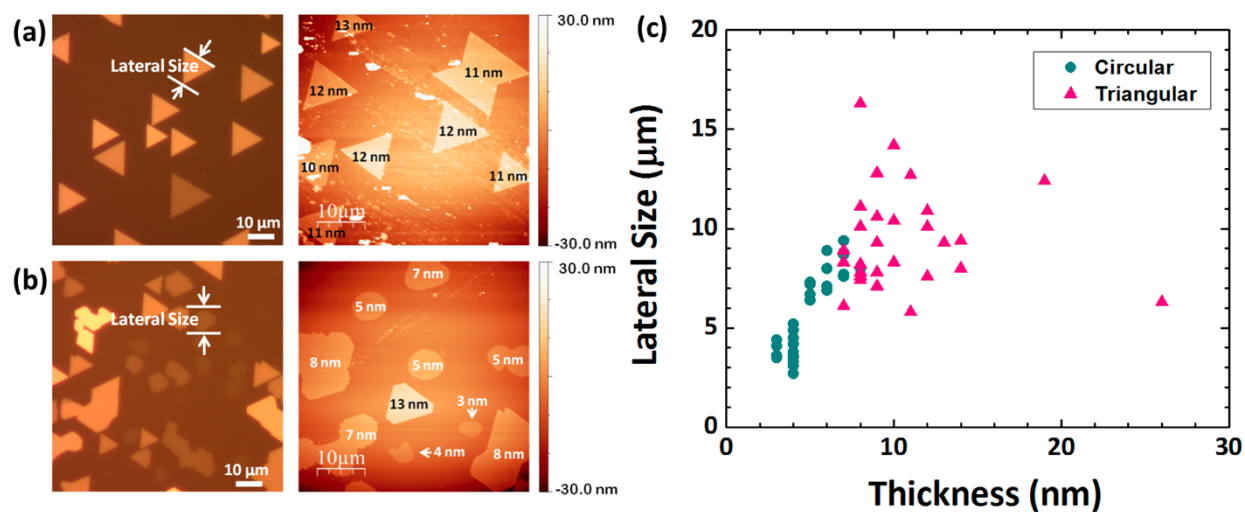


Figure S2. 2D nanosheet thickness and lateral size analysis. (a) Optical and AFM image of 2D nanosheets at the upstream area. (b) Optical and AFM image of 2D nanosheets at the downstream area. (c) Plot of the lateral size versus thickness of 28 triangular 2D nanosheets and 31 circular 2D nanosheets. The distance between the two areas for the statistical study is ~2 mm.

2. Microfabrication of porous SiO₂/Si substrates

The array of circular holes (diameter $2.0 \pm 0.2 \mu\text{m}$) was fabricated on a SiO₂/Si substrate by the standard photolithography/microfabrication processes in the class 100 (or ISO class 5) clean room at the University of Alabama. The silicon wafer (3", (100), n-type, As-doped, from University Wafers) was cut into samples of $\sim 0.5 \times 1.5 \text{ cm}$, which then were cleaned in the piranha solution at 120 °C for 10 minutes. The piranha solution was prepared as a 5:1 mixture of concentrated sulfuric acid (96 % H₂SO₄, from KMG Electronic Chemicals) with hydrogen peroxide (30 % H₂O₂, from KMG Electronic Chemicals). Hydrofluoric acid (48 % HF, from BDH Chemicals) was diluted, and the sample was treated with $\sim 5\%$ HF aqueous solution to remove native oxide. The safety protections and procedures were used/performed for using the piranha bath and HF bath for cleaning the sample. A layer of dry oxide was grown by annealing the sample at 1000 °C for $\sim 13 \text{ hrs}$ and 5 mins, under a pressure of 1 atm in the oxygen ambience (0.2 liter/min, high purity, from Airgas). The resulting dry oxide thickness was $\sim 270 \pm 3 \text{ nm}$, as confirmed by the optical reflectometry (Nanospec reflectometer, Nanometrics 212).

The sample was then spin-coated with Shipley 1811 photoresist (4000 rpm, 45 seconds), and then soft baked at 120 °C for 30 seconds. The hole array was created by using a mask aligner (Karl Suss MA6) with a corresponding pattern mask. The sample was exposed to UV light for 4.2 s, followed by 20s immersion in MF-319 developer (MICROPOSIT). The sample was then hard baked at 120 °C for 30 mins before proceeding to the ion milling. The ion milling (Intlvac Nanoquest Research Ion Beam Milling System) etched down the oxide to a depth of $\sim 165 \text{ nm}$, with a milling rate of $\sim 4.1 \text{ nm/min}$. The sample was then immersed in 1165 resist remover (MicroChem) at 80 °C for 24 hrs to strip off photoresist, then rinsed in de-ionized water baths 3 times, and finally blown dry with nitrogen. Before the 2D nanosheet transfer, the sample was

cleaned again in a piranha bath by following the standard procedures stated previously to ensure the removal of organic residues.

We notice that E and T could also be obtained for each individual 2D nanosheet if the non-linear stretching regime defined in Komaragiri *et al.*'s model is approached.²⁻⁴ The pre-strain parameter and the load parameter in this model were examined for the Bi₂Te₃ 2D nanosheet system (5 to 14 QLs) studied in this work, suggesting that even for the 5QL nanosheet group (*i.e.*, ~ 5 nm in thickness), the measured deformations were not entirely in the non-linear regime (*i.e.*, $F \sim \delta^3$). To reach the non-linear regime with reduced load parameters, it is needed to suspend 5~14QL nanosheets across holes with larger diameters. An alternative would be to suspend 1~3QL nanosheets. Such study is planned as part of a future publication.

3. 2D nanosheets transfer and suspension

The Bi₂Te₃ 2D nanosheet transfer method used in this study is based on recent progress made in transferring 2D nanosheets of graphene and other layered materials.⁵⁻⁷ The procedure is briefly illustrated in **Figure S3**. A ~240 nm thick film of poly(methyl methacrylate) (PMMA) (950 PMMA 4, from MicroChem) was spin-coated on the 2D nanosheet/mica substrate (3000 rpm for 1 min), and then baked at 180 °C for 5 mins (**Figure S3-2**). The PMMA film served as the sacrificial layer in this process. Then, acting as the carrier of the 2D nanosheets and the PMMA film, a piece of polydimethylsiloxane (PDMS, Sylgard 184, Dow Corning), ~1.5×1.5×0.3 cm, was brought in contact with the PMMA surface. When air bubbles were formed in the PDMS/PMMA interface, forces were gently and evenly applied to expel the bubbles. To detach the PMMA/2D nanosheets from the mica substrate, a droplet of water was applied at the interface of PMMA/mica (**Figure S3-3**). Due to the hydrophobicity of PMMA and the hydrophilicity of the mica substrate,⁵ water could quickly wet through the PMMA/mica interface as well as the 2D nanosheet/mica interfaces, leading to a detachment of the 2D nanosheets from the mica substrate. It should be noted that removing the nanosheets from the substrate without using the water wetting process was not possible, there was no indication of a 2D nanosheet detachment, indicating a strong van der Waals bonding between the 2D nanosheets and the mica substrate created in the heteroepitaxy process. Next, the PDMS with the PMMA film and the 2D nanosheets was peeled off slowly (**Figure S3-4**), and the 2D nanosheets were immediately brought in contact with the pre-fabricated porous substrate (**Figure S3-5**). To ensure direct surface contact between the PMMA and the SiO₂, the sample was baked on the hotplate at 50 °C for 30 mins. The sample was then subjected to acetone vapor for 30 minutes for partially dissolving PMMA, so the PDMS could be peeled off easily (**Figure S3-6**). To

improve the van der Waals bonding between the Bi_2Te_3 and the SiO_2 surfaces, the substrate was baked on the hotplate at $50\text{ }^\circ\text{C}$ for 30 mins. Finally, the PMMA film was then dissolved in a bath of acetic acid (Glacial, HPLC, from J.T.Baker) for 2 hrs, and then switched to a fresh acetic acid bath for the descum process. In the last step (**Figure S3-7**), the sample was immersed in ethanol, and then dried in carbon dioxide supercritical fluid (Denton DCP-1).

Figure S4 presents the optical images of the 2D nanosheets before and after the transfer. The 2D nanosheet transfer rate was shown to be extremely high ($\sim 98\%$). Yet, the current suspension yield drops sharply for 2D nanosheets < 5 QLs. It is speculated that those ultrathin nanosheets (1~4 QLs) might collapse during earlier transfer steps, instead of the final drying procedure. Improving this transfer process is still ongoing, which aims for ultrathin nanosheets for future investigations.

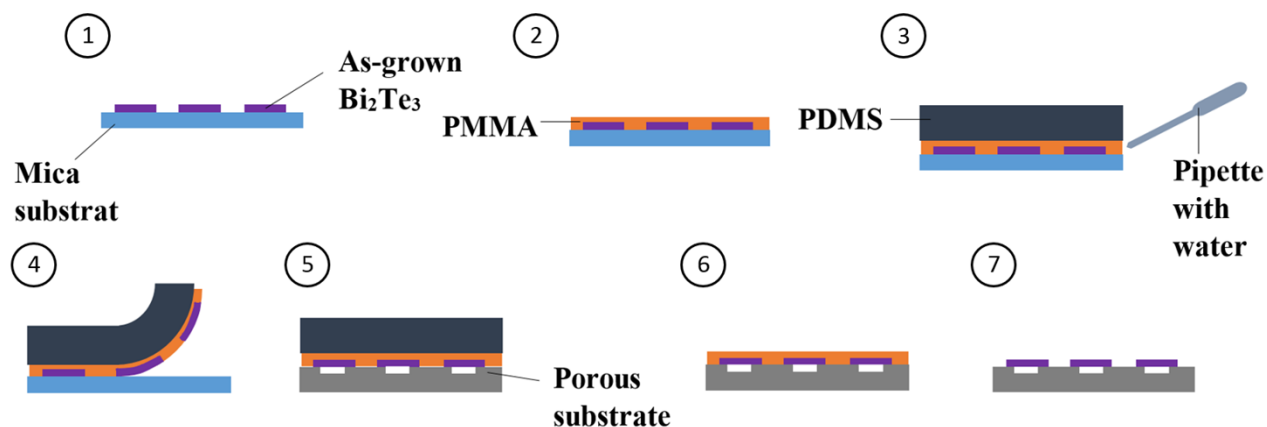


Figure S3. Flow chart of the 2D nanosheet transfer/suspension process.

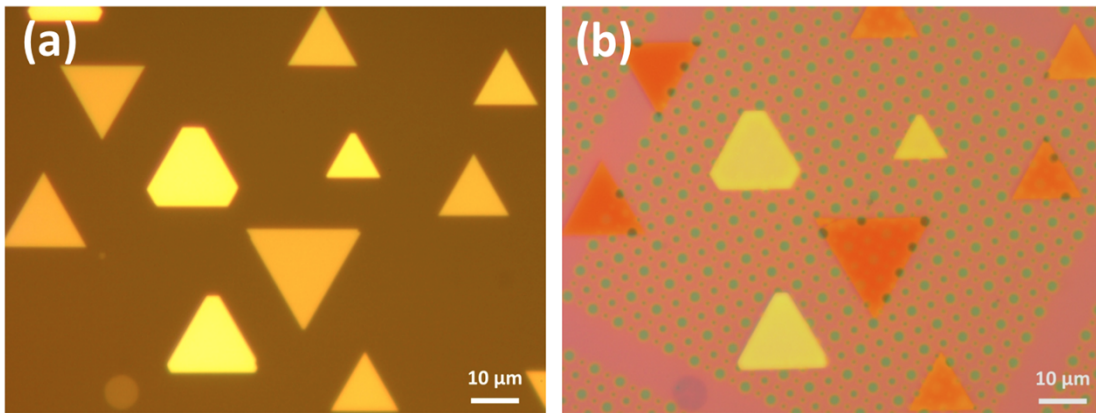


Figure S4. Optical image of the 2D nanosheets before and after the transfer.

4. Calibrations of AFM cantilever spring constants

The measurements of the AFM cantilever spring constants were based on the basic cantilever dimensions (i.e., Sader's model). The correlation for V-shaped cantilevers gives the expression:⁸

$$k = \frac{Ewt^3}{2L^3} \cos \theta \left[1 + \frac{4w^3}{b^3} (3 \cos \theta - 2) \right]^{-1}.$$

Where b is the width at the base of the “V”, θ is half the angle between the two legs, w is the width of the legs measured parallel to the front edge of the substrate, and L is the length of the cantilever measured straight out to the apex from the substrate. **Figure S5** presents the dimension measurements of the cantilever (DNP, vender provided $k \sim 0.35$ N/m, from Bruker) performed by the SEM (JEOL 7000). The spring constant of the AFM cantilever was obtained as 0.19 ± 0.05 N/m, where the error ($\sim 26\%$) is mainly due to the uncertainty of the elastic modulus (E) of the silicon nitride, provided by the vendor (210 N/m).⁹

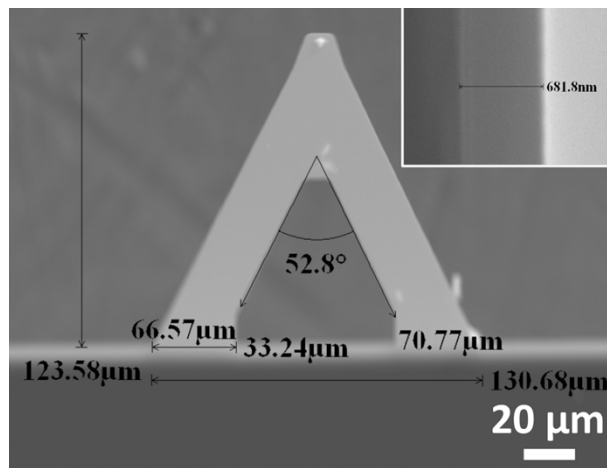


Figure S5. The dimension measurements for the V-shape cantilever. Inset is the cross-sectional image of the thickness of the cantilever.

5. AFM tip radius measurements

The requirement for adopting this model for small and finite size indenter is that the radius of the tip (r_{tip}) should be greatly less than r .² As shown in **Figure S6**, The r_{tip} in this work was measured to find 26.8 ± 2.6 nm using a scanning electron microscope (SEM, JEOL 7000), and the resultant r_{tip}/r is in the range of 0.026 to 0.028, which validates the adoption of Komaragiri *et al.*'s model for this work.

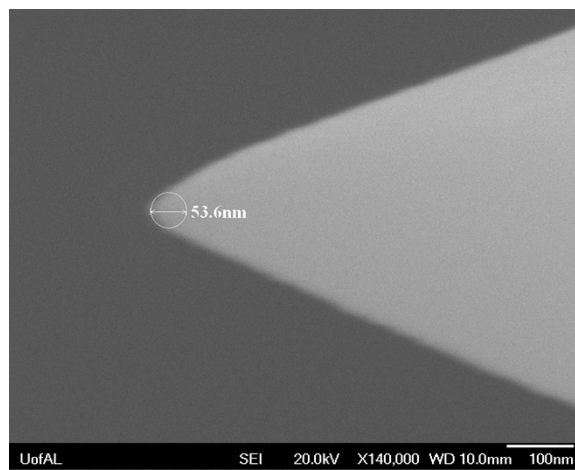


Figure S6. SEM image of the AFM tip with a radius of 26.8 ± 2.6 nm.

6. List of the data reported

Figure S7 to S10 are the AFM images and the k_{2D} values of all 26 samples, and Figure S11 presents the cross-section profiles of the 5-QL, 6-QL, 8-QL, and 14-QL nanosheets. These data were used to acquire Figure 3 that was then used for determining the overall E and T of the Bi_2Te_3 2D nanosheets.

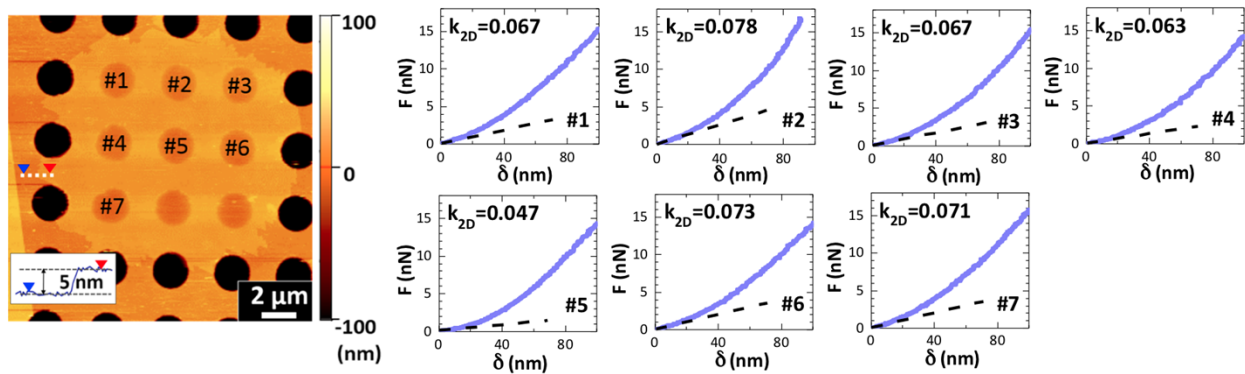


Figure S7. The AFM topography image of the 5-QL nanosheet and the $F(\delta)$ curves of the tested freestanding circular nanosheets.

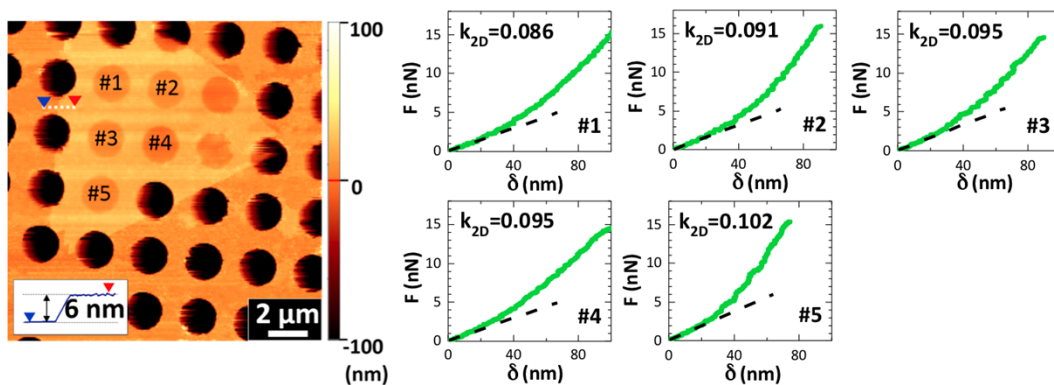


Figure S8. The AFM topography image of the 6-QL nanosheet and the $F(\delta)$ curves of the tested freestanding circular nanosheets.

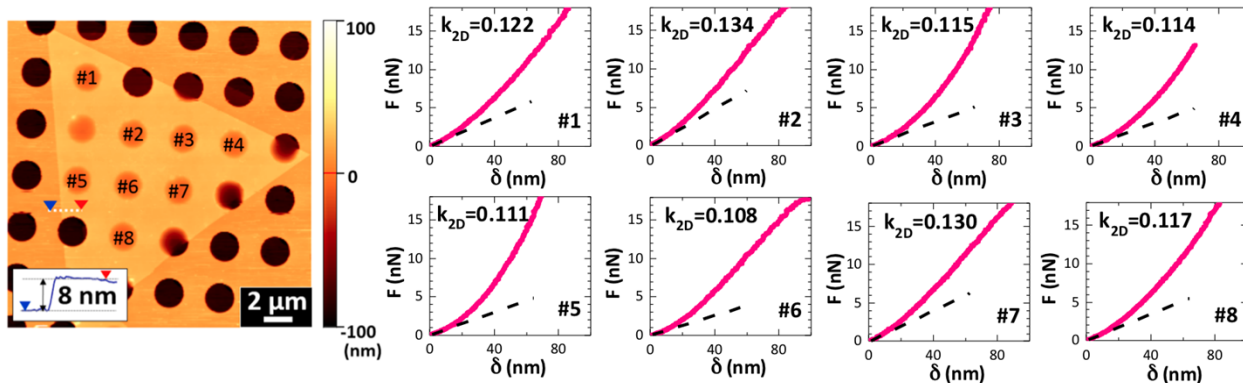


Figure S9. The AFM topography image of the 8-QL nanosheet and the $F(\delta)$ curves of the tested freestanding circular nanosheets.

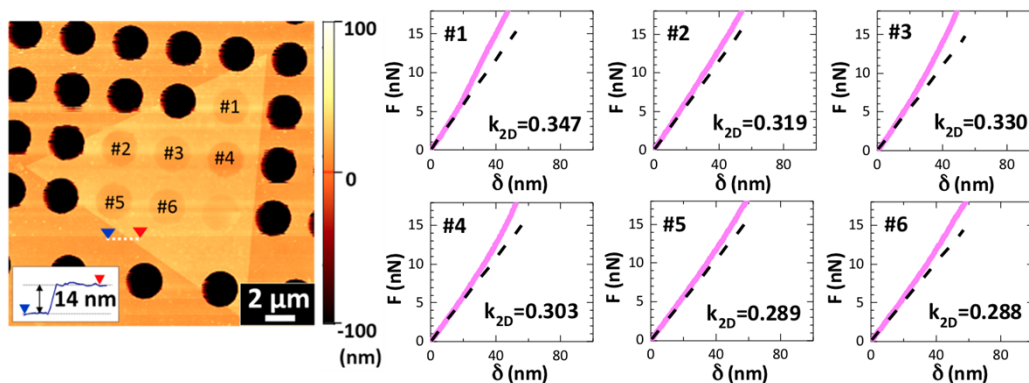


Figure S10. The AFM topography image of the 14-QL nanosheet and the $F(\delta)$ curves of the tested freestanding circular nanosheets.

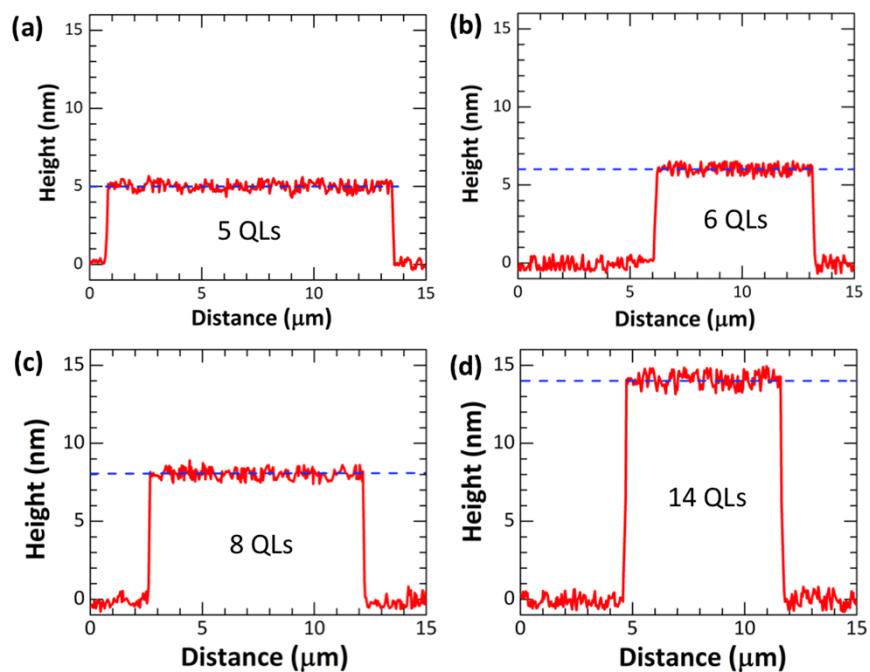


Figure S11. The AFM cross-section profiles of the four 2D nanosheets. The thicknesses/errors are $5 \text{ nm} \pm 0.5 \text{ nm}$ for 5 QLs, $6 \text{ nm} \pm 0.5 \text{ nm}$ for 6 QLs, $8 \text{ nm} \pm 0.6 \text{ nm}$ for 8 QLs, and $14 \text{ nm} \pm 0.8 \text{ nm}$ for 14 QLs.

7. References cited

1. H. Li, J. Cao, W. Zheng, Y. Chen, D. Wu, W. Dang, K. Wang, H. Peng and Z. Liu, *Journal of the American Chemical Society*, 2012, **134**, 6132-6135.
2. C. Lee, X. Wei, J. W. Kysar and J. Hone, *Science*, 2008, **321**, 385-388.
3. U. Komaragiri, M. R. Begley and J. G. Simmonds, *Journal of Applied Mechanics*, 2005, **72**, 203-212.
4. S. Bertolazzi, J. Brivio and A. Kis, *ACS Nano*, 2011, **5**, 9703-9709.
5. H. Li, J. Wu, X. Huang, Z. Yin, J. Liu and H. Zhang, *ACS Nano*, 2014, **8**, 6563-6570.
6. M. Her, R. Beams and L. Novotny, *Physics Letters A*, 2013, **377**, 1455-1458.
7. A. Reina, H. Son, L. Jiao, B. Fan, M. S. Dresselhaus, Z. Liu and J. Kong, *The Journal of Physical Chemistry C*, 2008, **112**, 17741-17744.
8. J. E. Sader, *Review of Scientific Instruments*, 1995, **66**, 4583-4587.
9. B. Ohler, *Practical Advice on the Determination of Cantilever Spring Constants*, Veeco Instruments Inc., 2007.